ISSN 0036-0236, Russian Journal of Inorganic Chemistry, 2024, Vol. 69, No. 3, pp. 359–365. © Pleiades Publishing, Ltd., 2024.

STRUCTURE, MAGNETIC AND OPTICAL PROPERTIES OF MATERIALS

Luminescent Mn^{2+}-Doped $MgO–Al_2O_3–ZrO_2–SiO_2$ Sol–Gel Materials

S. K. Evstropiev[a, b, c, *], V. L. Stolyarova[d, e], A. S. Saratovskii[c, d], D. V. Bulyga[a, b], K. V. Dukelskii[a, b, f], N. B. Knyazyan[g], and D. A. Yurchenko[d]

[a] *Vavilov State Optical Institute», St. Petersburg, 192171 Russia*

[b] *ITMO University, St. Petersburg, 197101 Russia*

[c] *St. Petersburg State Institute of Technology, St. Petersburg, 190013 Russia*

[d] *Grebenshchikov Institute of Silicate Chemistry, St. Petersburg, 199034 Russia*

[e] *St. Petersburg State University, St. Petersburg, 199034 Russia*

[f] *Bonch-Bruevich St. Petersburg State University of Telecommunications, St. Petersburg, 193232 Russia*

[g] *Armenian State Institute of Inorganic Chemistry, Yerevan, 0051 Armenia*

**e-mail: evstropiev@bk.ru*

Received September 19, 2023; revised December 11, 2023; accepted December 12, 2023

Abstract—Mn^{2+}-doped $MgO–Al_2O_3–ZrO_2–SiO_2$ materials have been synthesized by the sol–gel method, and their structure, morphology, chemical composition, and luminescent properties have been studied using X-ray diffraction, scanning electron microscopy, EDX analysis, and luminescence spectroscopy. The sol–gel method has been shown to ensure high homogeneity of the chemical composition over the volume of the synthesized materials. The introduction of Mn into the composition of sol–gel materials significantly accelerates crystallization processes in them during heat treatment. The luminescence spectra of the materials display several groups of emission bands in the blue and yellow-red parts of the visible spectral range. The resulting materials are promising for use as phosphors in the lighting for plant production.

Keywords: defects, manganese, aluminum-magnesium spinel

DOI: 10.1134/S0036023623603446

Various luminescent Mn^{2+}-doped oxide materials have wide practical applications [1–12]. Mn^{2+} ions can occupy different structural positions in these materials ($[MnO_4]$ or $[MnO_6]$), and the spectral and luminescent properties of these ions are very sensitive to the structure of their nearest environment [8–16]. This determines the efficiency of using Mn^{2+} ions as a component of various luminescent materials.

The splitting of the electronic levels of Mn^{2+} under the influence of the crystal field of the nearest environment determines the features of the spectral and luminescent properties of these ions in solid matrices. The Tanabe–Sugano diagram [17] is often used to describe this phenomenon in various matrices [4, 12, 15–19].

Figure 1 shows an illustrative Tanabe–Sugano diagram, constructed on the basis of data from [18, 20] and demonstrating the influence of the crystal field strength (CFS) on the splitting of energy levels of Mn^{2+} ions. According to the Tanabe–Sugano diagram, the spectral position of the emission band of the Mn^{2+} ion depends on the strength of the crystal field of its surroundings. The CFS of Mn^{2+} ions in a tetrahedral environment is noticeably weaker than that in an octahedral environment [12, 20].

Figure 1 shows that the luminescence bands of Mn^{2+} ions in both structural positions are associated with the electronic transition $^4T_1(G) \rightarrow {}^6A_1(S)$, but these bands are in different ranges of the visible spectrum. The Mn^{2+} ions in a tetrahedral coordination (Mn^{2+}(IV)) exhibit green emission [15, 16, 20–22], while ions in an octahedral coordination ((Mn^{2+}(VI)) luminesce in the yellow-red range of the spectrum [18, 20, 23, 24]. The authors of [25] also observed luminescence under the influence of UV radiation (λ_{ex} = 356 nm) in $CaYAl_3O_7$:Mn^{2+} crystals in the near-UV and blue ranges of the spectrum (bands with λ_{max} = 389 and 412 nm) and attributed it to the emission of Mn^{2+} ions.

At the same time, the introduction of Mn^{2+} ions into the crystal lattice of oxide materials leads to its distortion [26, 27] and the formation of structural defects, which affects the luminescent properties of materials [24, 27, 28]. In this case, luminescent centers in Mn^{2+}-doped materials can be both intrinsic

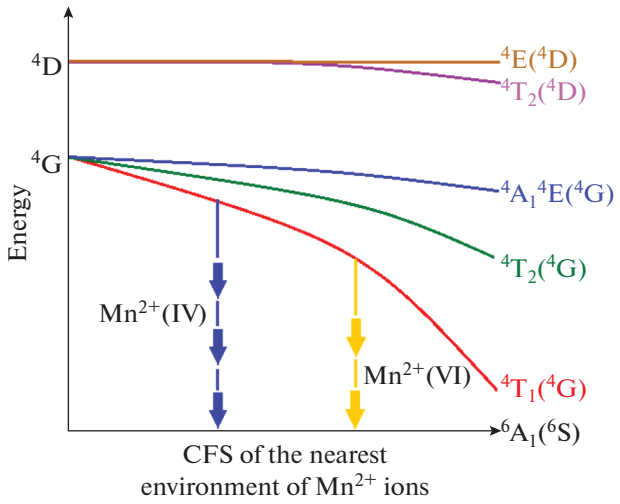

Fig. 1. Illustrative Tanabe–Sugano diagram constructed on the basis of data from [18, 20] and demonstrating the influence of the strength of the crystal field of the nearest environment on the splitting of energy levels of Mn^{2+} ions.

structural defects of the oxide matrices [22, 24, 27] and manganese ions [28, 29].

Various silicate glass-ceramics containing additives of manganese compounds have been synthesized and studied [1–3, 10, 11, 13, 20, 30]. It has been shown that these materials are promising for use as luminescent radiation converters in white LEDs [30]. It is known that many glass-ceramic materials contain several types of crystals [12, 31, 32], and structural design opens new opportunities for fabricating materials with luminescence bands in different spectral ranges [10].

In addition, Mn^{2+} ions found in some matrices, for example, in $MgAl_2O_4$, can be oxidized to give Mn^{4+} ions, which replace Al^{3+} ions and have luminescence bands in the red range of the spectrum [15, 33, 34].

This approach is relevant for the development of luminescent materials that are promising for special lighting systems used in crop production. It is known that to accelerate plant growth, lamps have been developed and used that emit in two spectral ranges: in the blue and red ranges of the spectrum [35–37]. Considering the above-described features of the luminescent properties of Mn^{2+} ions, glass-ceramic materials in which these ions are embedded in various crystals and are in them in both tetrahedral and octahedral coordination can be promising for plant growing lighting technology.

The efficiency of using phosphors of the $Ba_{1.3}Sr_{1.7}MgSi_2O_8$ system containing two activator ions (Eu^{2+} and Mn^{2+}) as a component of glass-ceramic composites for agricultural lighting systems was experimentally demonstrated in [37]. The use of lamps based on these phosphors has been shown to increase the yield of the vegetable crop Romaine lettuce by more than 50% compared to commercial greenhouse lamps. It should be noted, however, that the content of the rare earth component (Eu) in the phosphors developed in [37] is 6%, and this determines their rather high cost and the relevance of developing materials for technological lighting systems in greenhouses that do not contain expensive components.

Crystallization of glasses in the $MgO–Al_2O_3–SiO_2$ system leads to the formation of glass-ceramic materials containing various crystals [31, 32, 38]. These materials can be considered a glass-ceramic matrix for introducing Mn^{2+} ions into it [3], have high thermal stability and mechanical strength, and are used in various optical applications [31, 32, 38, 39]. By introducing cobalt compounds into the composition of these materials, heat-resistant light filters and passive Q switches were obtained [39].

The ionic radii of Mg^{2+} and Mn^{2+} are close (0.72 and 0.83 Å, respectively [40]), and Mn^{2+} can replace Mg^{2+} in the structure of many crystals [15, 41, 42]. It has been shown [3] that the introduction of MnO into the composition of glass-ceramic materials of the $MgO–Al_2O_3–SiO_2$ system additionally increases their high mechanical strength. In this work, it has been established that the introduction of manganese oxide somewhat changes the crystal structure of glass ceramics.

The crystalline phases formed upon the crystallization of glasses of the $MgO–Al_2O_3–SiO_2$ system (aluminum magnesium spinel; quartz-like solid solutions) can contain intrinsic structural defects that determine the luminescence of materials in the near-UV and blue parts of the spectrum. In particular, aluminum magnesium spinel under short-wave UV light shows intense luminescence bands with maxima at 316, 380, 400, and 460 nm [43]. In this spectral range, luminescence of structural defects characteristic of silica obtained by the sol–gel route, described in detail in [44], can also be observed. In addition, studying the luminescent properties of aluminosilicate glasses presented in [29] indicates a high efficiency (>85%) of excitation energy transfer from structural defects $[SiO_{4-x}]$ to Mn^{2+} ions. Based on the literature data, we can conclude that the study of Mn^{2+}-doped $MgO–Al_2O_3–SiO_2$ materials is relevant.

The present work focuses on the synthesis and study of Mn^{2+}-doped $MgO–Al_2O_3–ZrO_2–SiO_2$ materials, which do not contain expensive rare-earth components. The traditional method of glass melting for this system and subsequent production of glass-ceramic materials requires the use of high synthesis temperatures, so that it is difficult to obtain homogeneous samples using this method. Therefore, in this work, a low-temperature sol–gel method was used to obtain Mn^{2+}-doped $MgO–Al_2O_3–ZrO_2–SiO_2$ materials.

EXPERIMENTAL

The materials were synthesized by the sol–gel method using soluble metal salts and tetraethoxysilane (TEOS). Aqueous solutions of $Mg(NO_3)_2$, $Al(NO_3)_3$, $ZrOCl_2$, and $MnSO_4$ in a given ratio were mixed at room temperature with TEOS, dimethylformamide, and 2-propanol.

After gelation, the material samples were dried at 70°C in an oven and subjected to heat treatment in an electric muffle furnace for 2 h at temperatures of 600, 900, or 1150°C. The chemical composition of the materials is presented in Table 1. Gel **1** was synthesized without the addition of manganese, and gel **2** contained manganese.

The crystal structure of the resulting powders was studied by powder X-ray diffraction analysis on a Rigaku Ultima IV X-ray diffractometer. The morphology of powder grains was studied using a Vega3 Tescan scanning electron microscope equipped with an Oxford Instruments Advanced Aztec Energy unit for energy-dispersive X-ray analysis. Luminescence and luminescence excitation spectra were measured on a Perkin Elmer LS 50B spectrofluorimeter.

Table 1. Chemical composition of the synthesized oxide composites (mol %)

Sample	MgO	Al_2O_3	SiO_2	MnO
1	11.2	16.5	72.3	–
2	9.9	16.9	68.8	4.4

The nominal chemical composition of the composites, expressed in elemental oxides and calculated from the chemical composition of the sols, is given.

RESULTS AND DISCUSSION

Figure 2 shows X-ray diffraction patterns of samples heat-treated at various temperatures. It is seen that the initial gels and powders calcined at 600°C are amorphous. Heat treatment at 1150°C leads to the formation of various crystalline phases: cordierite, enstatite, ZrO_2, and β-quartz solid solutions. It is known that these crystals often form during the crystallization of glasses of the $MgO–Al_2O_3–ZrO_2–SiO_2$ system and the formation of glass-ceramics [3, 32]. Note that the nature of the thermal evolution of the crystal structure of materials synthesized by the sol–gel method is similar to the changes observed during the crystallization of $MgO–Al_2O_3–ZrO_2–SiO_2$ glasses described in [32].

Comparison of Figs. 2a and 2b shows that the introduction of manganese into the composition of materials leads to a considerable acceleration of crystallization processes in them. The significant influence of manganese additives on the crystallization processes of silicate materials has been reported earlier [3, 41].

Figures 3 and 4 show SEM images of initial gels **1** and **2** (Figs. 3a, 4) and gels heat-treated at 600°C (Fig. 4b), 900°C (Fig. 4c), and 1150°C (Figs. 3b, 4d). The initial gels contain large, irregularly shaped aggregates consisting of submicron particles 100–200 nm in size. The particle size in powders changes noticeably with increasing heat treatment temperature, and the structure of heat-treated gels consists of submicron particles.

Figure 5 shows the photoluminescence and luminescence excitation spectra of glass-crystalline material **2** obtained after heat treatment at (a) 900 and (b) 1150°C. The luminescence spectrum shows emission bands in the blue (λ_{max} ~ 410 nm) and yellow-red (λ_{max} = 560–640 nm) spectral ranges. The observed

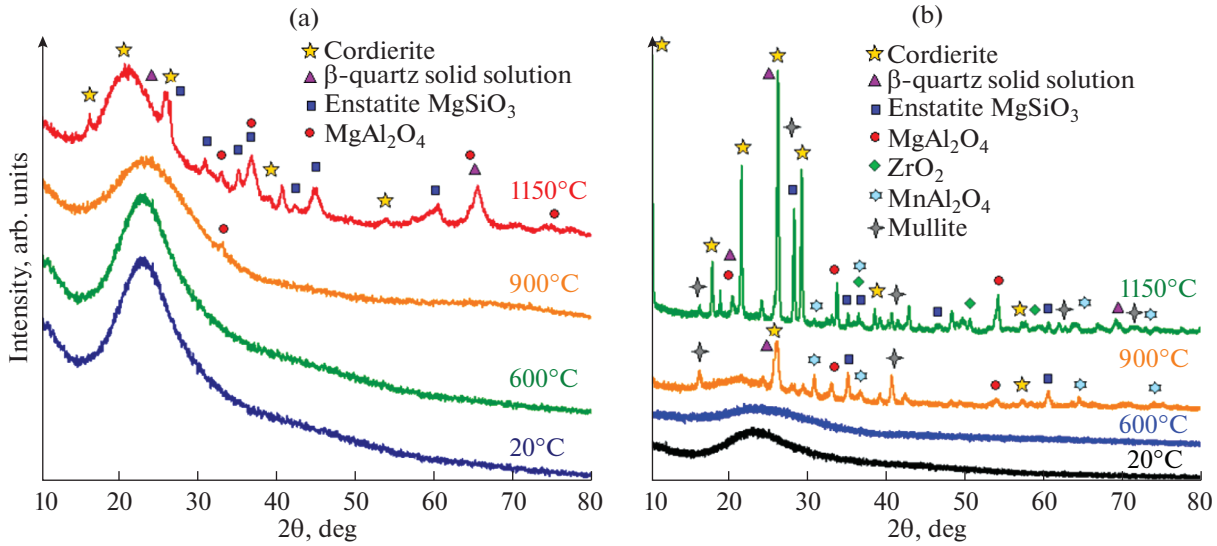

Fig. 2. X-ray diffraction patterns of sol–gel powders of the $MgO–Al_2O_3–ZrO_2–SiO_2$ system obtained from (a) gel **1**, not containing Mn, and (b) Mn-doped gel **2** heat treated at different temperatures.

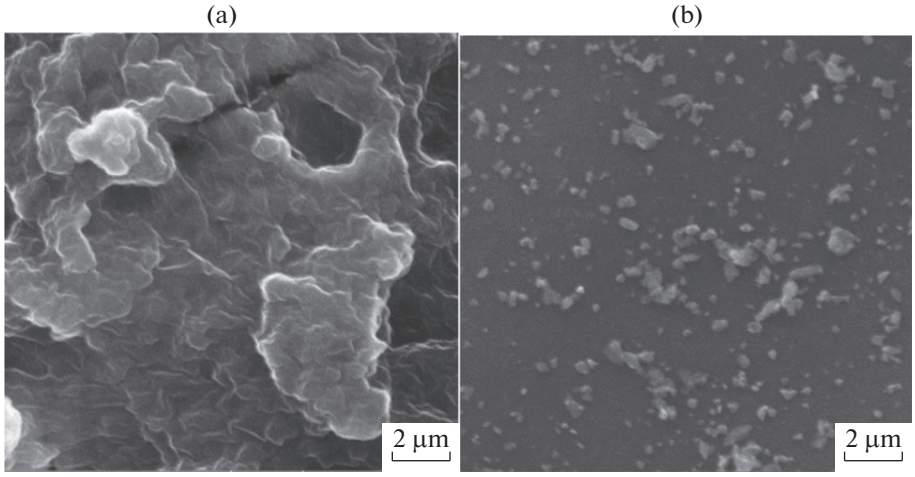

Fig. 3. SEM images of gel **1**, not containing Mn: (a) initial gel before heat treatment and (b) gel **1** heat treated at 1150°C.

shape of the emission bands suggests that they have a complex structure and are the result of the superposition of several luminescence bands of different intensities. The large number of different crystalline phases in the structure of the obtained materials (Fig. 2), the variability of the valence and coordination state of manganese ions, and the mutual overlap of various emission bands in the spectra make their identification difficult.

The strongest luminescence band with $\lambda_{max} \sim 410$ nm (Figs. 5a, 5b, curve *1*) is observed when the material is excited under UV-C light ($\lambda_{ex} = 250$ nm). According to [22], the excitation of luminescence (Fig. 5a, 5b, curve 1) by UV-C light is related to the fundamental absorption of the matrix.

Crystals formed during the crystallization of materials of the $RO–Al_2O_3–SiO_2$ system (aluminum magnesium spinel; quartz-like solid solutions) can have intrinsic structural defects that determine the luminescence of the materials in the near-UV and blue ranges of the spectrum. For example, the luminescence spectra of aluminum magnesium spinel excited by short-wave UV light show strong bands with maxima at 316, 380, 400, and 460 nm [43]. This spectral range can also display the luminescence of structural defects described in detail in [44], characteristic of silica obtained by the sol–gel method. These data allow us to assume that structural defects in the resulting materials make the major contribution to the luminescence observed in the blue part of the spectrum.

A green luminescence band with a maximum at 525 nm, corresponding to Mn^{2+} in a tetrahedral environment, was observed in $MgAl_2O_4$ crystals upon excitation with blue light [15, 45]. The quantum efficiency of luminescence, according to [45], was quite high (45%). In the present work, we also observe luminescence bands in the green-yellow part of the spectrum (Figs. 5a, 5b), but their intensity is low. This phenomenon can be explained by the relatively small content of spinel crystals in the structure of the resulting material.

In Mn^{2+}-doped oxide materials, luminescence excitation in green ($\lambda \sim 500–540$ nm; Figs. 5a, 5b, curve *2*) and yellow-red ($\lambda \sim 560–660$ nm; Fig. 5a, curves *3*, *4*; Fig. 5b, curves *3–5*) spectral ranges are determined by the absorption bands of Mn^{2+} ions associated with electronic transitions from the $^6A_1(^6S)$ level to the $^4T_2(^4G)$, $[^4A_1(^4G)$, $^4E(^4G)]$, $^4E(^4D)$, and $^4T_2(D)$ levels (Fig. 1) [20]. In addition, the emission observed in the red range of the spectrum can be associated with the partial oxidation of Mn^{2+} ions and the entry of the resulting Mn^{4+} ions into the lattice of spinel crystals [15, 33, 34]. At the same time, red luminescence can be due to the presence of structural defects in silica [44].

Comparison of emission bands (Figs. 5a, 5b, curves *1*, *2*) in the blue range of the spectrum ($\lambda = 400–460$ nm) with luminescence excitation bands in the yellow-red region of the spectrum (Fig. 5a, curves *5*, *6*; Fig. 5b, curve *6*) shows their significant overlap. This suggests the possibility of transfer of excitation energy between different luminescent centers or reabsorption of radiation in the material.

Figure 5c illustrates changes in the emission spectra of gel **2** with an increase in the temperature of its heat treatment from 900 to 1150°C. An increase in the heat treatment temperature, leading to the development of crystallization processes in the material (Fig. 2), determines an almost identical increase in luminescence intensity in the blue and green-yellow regions of the spectrum. The comparison of the difference spectra shown in this figure and the luminescence spectra shown in Figs. 5a and 5b demonstrates that the emission peaks have the same spectral position. This allows us to conclude that increasing heat treatment temperature leads to an increase in the concentration of already formed luminescent centers.

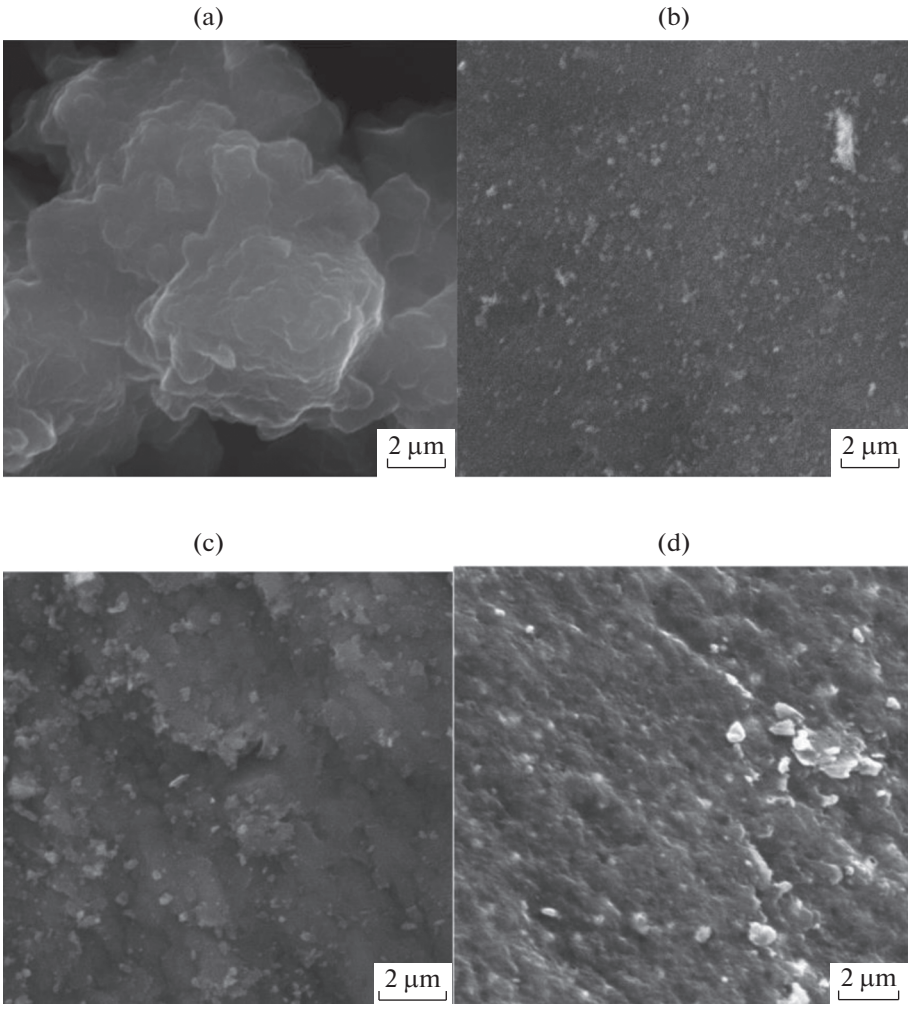

Fig. 4. SEM images of Mn-doped gel **2**: (a) initial gel before heat treatment and (b–d) gel heat treated at (b) 600, (c) 900, and (d) 1150°C.

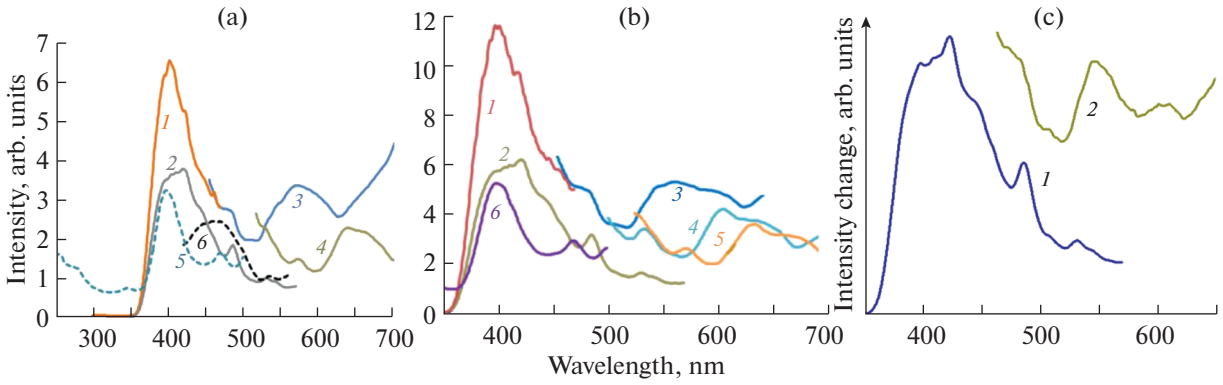

Fig. 5. (a) Emission (*1*–*4*) and luminescence excitation (*5*, *6*) spectra of gel **2** heat treated at 900°C. The luminescence excitation wavelength: (*1*) 250, (*2*) 350, (*3*) 400, and (*4*) 480 nm. The emission wavelength: (*5*) 560 and (*6*) 640 nm. (b) Emission (*1*–*5*) and luminescence excitation (*6*) spectra of gel **2** heat treated at 1150°C. The luminescence excitation wavelength: (*1*) 250, (*2*) 300, (*3*) 400, (*4*) 450, and (*5*) 480 nm. The emission wavelength: (*6*) 560 nm. (c) Difference emission spectra (excitation wavelength (*1*) 350 and (*2*) 400 nm) of gel **2**, which demonstrate changes in emission spectra of the gel with increasing heat treatment temperature from 900 to 1150°C.

Figure 5 shows that the resulting glass-ceramic materials based on the $MgO–Al_2O_3–ZrO_2–SiO_2$ system exhibit a combination of blue ($\lambda \sim 410–425$ nm) and yellow-red ($\lambda \sim 560–660$ nm) luminescence, which is optimal for their use in agricultural lighting systems to stimulate plant growth and development [36, 37]. The use of these heat-resistant, chemically stable, and inexpensive luminescent materials as phosphors in lighting technology of crop production is very promising.

CONSLUSIONS

Mn^{2+}-doped $MgO–Al_2O_3–ZrO_2–SiO_2$ materials have been synthesized by the sol–gel method, and their morphology, structure, and luminescent properties have been studied. The introduction of Mn into the composition of materials significantly accelerates the crystallization processes during heat treatment of materials up to 1150°C. The use of Mn^{2+}-doped luminescent materials of the $MgO–Al_2O_3–ZrO_2–SiO_2$ system as phosphors in lighting technology of plant production is very promising.

FUNDING

This work was supported by ongoing institutional funding. No additional grants to carry out or direct this particular research were obtained.

CONFLICT OF INTEREST

The authors of this work declare that they have no conflicts of interest.

REFERENCES

1. K. Omri and F. Alharbi, J. Mater. Sci.: Mater. Electron. **32**, 12466 (2021). https://doi.org/10.1007/s10854-021-05880-z
2. R. Geng, B. Zhou, J. Wang, et al., J. Am. Ceram. Soc. **105**, 4709 (2022). https://doi.org/10.1111/jace.18447
3. B. Li, Q. Xia, and Z. Wang, J. Australian Ceram. Soc. **57**, 927 (2021). https://doi.org/10.1007/s41779-021-00588-z
4. W. Ran, L. Wang, Q. Liu, et al., RSC Adv. **7**, 17612 (2017). https://doi.org/10.1039/C7RA01623A
5. B. Lei, Y. Liu, Z. Ye, and C. Shi, J. Lumin. **109**, 215 (2004). https://doi.org/10.1016/j.jlumin.2004.02.010
6. V. Lojpur, M. G. Nikolić, D. Jovanović, et al., Appl. Phys. Lett. **103**, 141912 (2013). https://doi.org/10.1063/1.4824208
7. W.-R. Liu, C.-H. Huang, C.-W. Yeh, et al., RSC Adv. **3**, 9023 (2013). https://doi.org/10.1039/c3ra40471d
8. W. Liu, Q. Lin, H. Li, et al., J. Am. Chem. Soc. **138**, 14954 (2016). https://doi.org/10.1021/jacs.6b08085
9. X. Xu, Y. Xing, and Z. Yang, Mater. Res. Express **9**, 015202 (2022). https://doi.org/10.1088/2053-1591/ac4b50
10. Z. Fang, W. Peng, S. Zheng, et al., J. Eur. Ceram. Soc. **40**, 1658 (2020). https://doi.org/10.1016/j.eurceramsoc.2019.12.025
11. P. Li, M. Peng, L. Wondraczek, et al., J. Mater. Chem. C **3**, 3406 (2015). https://doi.org/10.1039/C5TC00047E
12. S. K. Batygov, M. N. Brekhovskikh, L. V. Moiseeva, et al., Inorg. Mater. **55**, 1185 (2019). https://doi.org/10.1134/S0020168519110025
13. J. Qiu, H. Igarashi, and A. Makishima, Sci. Technol. Adv. Mater. **6**, 431 (2005). https://doi.org/10.1016/j.stam.2004.12.002
14. O. B. Tomilin, E. E. Muryumin, and M. V. Fadin, Russ. J. Inorg. Chem. **68**, 256 (2023). https://doi.org/10.1134/S0036023622602616
15. N. M. Khaidukov, M. N. Brekhovskikh, N. Y. Kirikova, et al., Russ. J. Inorg. Chem. **65**, 1135 (2020). https://doi.org/10.1134/S0036023620080069
16. M. N. Brekhovskikh, S. K. Batygov, L. V. Moiseeva, et al., Russ. J. Inorg. Chem. **67**, 1855 (2022). https://doi.org/10.1134/S0036023622600733
17. Y. Tanabe and S. Sugano, J. Phys. Soc. Jpn. **9**, 776 (1954). . https://doi.org/10.1143/JPSJ.9.766
18. Y. Zhuang, J. Ueda, and S. Tanabe, Appl. Phys. Lett. **105**, 191904 (2014). https://doi.org/10.1063/1.4901749
19. M. Czaja, R. Lisiecki, R. Juroszek, et al., Minerals **11**, 1215 (2021). https://doi.org/10.3390/min11111215
20. S. Lin, H. Lin, C. Ma, et al., Light: Sci. Appl. **9**, 22 (2020). . https://doi.org/10.1038/s41377-020-0258-3
21. T. E. Warner, M. M. Bancells, P. Brilner Lund, et al., J. Solid State Chem. **277**, 434 (2019). https://doi.org/10.1016/j.jssc.2019.06.038
22. A. Luchenko, Y. Zhydachevskyy, S. Ubizskii, et al., Sci. Rep. **9**, 9544 (2019). https://doi.org/10.1038/s41598-019-45869-7
23. Wei Donglei and Seo Hyo Jin, J. Mater. Chem. C **8**, 7899 (2020). https://doi.org/10.1039/D0TC01143F
24. C. F. Yu and P. Lin, J. Appl. Phys. **79**, 7191 (1996). https://doi.org/10.1063/1.361435
25. A. Selot, J. Tripathi, S. Tripathi, et al., Luminescence **29**, 362 (2014). https://doi.org/10.1002/bio.2553
26. O. Bilgili, Acta Physica Polonica A **136**, 460 (2019).
27. A. Dhanalakshmi, B. Natarajan, V. Ramadas, et al., Pramana J. Phys. **87**, 57 (2016). https://doi.org/10.1007/s12043-016-1248-0
28. Q. Hu, Z. Gao, X. Lu, et al., J. Mater. Chem. C **5**, 11806 (2017). https://doi.org/10.1039/c7tc04020b

29. Z. Hua, G. Tang, Q. Wei, et al., Int. J. Appl. Glass Sci. **14**, 573 (2023). https://doi.org/10.1111/ijag.16640
30. N. Da, M. Peng, S. Krolikowski, et al., Opt. Express **18**, 2549 (2010). https://doi.org/10.1364/OE.18.002549
31. S. K. Evstropiev, D. A. Yurchenko, V. L. Stolyarova, et al., Ceram. Int. **48**, 24517 (2022). https://doi.org/10.1016/j/ceramint.2022.05.090
32. A. V. Bortkevich, O. S. Dymshits, A. A. Zhilin, et al., J. Opt. Technol. **69**, 558 (2002).
33. N. M. Khaidukov, M. N. Brekhovskikh, N. Yu. Kirikova, et al., Opt. Spektr. **131**, 450 (2023). https://doi.org/10/21883/OS.2023.04.55547.56-22
34. N. M. Khaidukov, M. N. Brekhovskikh, N. Yu. Kirikova, et al., Ceram. Int. **46**, 21351 (2020). https://doi.org/10.1016/j.ceramint.2020.05.231
35. A. Yano and K. Fujiwara, www.plantmethods.com/content/8/1/46
36. L. B. Prikupets, Svetotekhnika **6**, 6 (2017).
37. W. Chen, X. Zhang, J. Zhou, et al., J. Mater. Chem. C **8**, 3996 (2020). https://doi.org/10.1039/dotc00061b
38. D. A. Yurchenko, S. K. Evstropiev, A. V. Shashkin, et al., Dokl. Chem. **499**, 159 (2021). https://doi.org/10.1134/S0012500821080048
39. Yu. V. Volk, I. A. Denisov, and A. M. Malyarevich, Appl. Opt. **43**, 682 (2004). https://doi.org/10.1364/AO.43.000682
40. R. D. Shannon, Acta Crystallogr., Sect. A **32**, 751 (1976).
41. M. Catalano, A. Bloise, V. Pingitore, et al., Cryst. Res. Technol. **49**, 736 (2014). https://doi.org/10.1002/crat.201400102
42. C. Dlamini, M. R. Mhlongo, L. F. Koao, et al., Appl. Phys. A **126**, 75 (2020). https://doi.org/10.1007/s00339-019-3248-7
43. Y.-K. Wang, X. Xie, and C.-G. Zhu, ACS Omega **7**, 1267 (2022). https://doi.org/10.1021/acsomega.1c06583
44. R. Salh, *Silicon Nanocluster in Silicon Dioxide: Cathodoluminescence, Energy Dispersive X-Ray Analysis, Infrared Spectroscopy Studies, Crystalline Silicon*, Ed. by Basu S. (Properties and Uses, 2011). ISBN 978-953-307-587-7.
45. E. Song, Y. Zhou, Y. Wei, et al., J. Mater. Chem.C **7**, 8192 (2019). https://doi.org/10.1039/C9TC02107/1

Translated by G. Kirakosyan

SPELL: OK